

Bachelor Thesis  
Biomedical Engineering  
Multi-Modality Medical Imaging (M3I)  
Marthe Mom (s2822741)  
December 2, 2024

# Development of a fibroglandular tissue phantom for testing and validation of dynamic contrast-enhanced dedicated breast CT

**UNIVERSITY  
OF TWENTE.**

Chair: prof.dr. Ioannis Sechopoulos  
Daily supervisor: Liselot Goris, MSc  
External member: dr. Vincent Groenhuis

## Abstract

Dynamic contrast-enhanced dedicated breast computed tomography (DCE-bCT) is a new imaging modality for diagnosis, treatment planning and response monitoring of breast cancer. To validate and optimise the acquisition and reconstruction parameters for this modality, a fibroglandular tissue perfusion phantom is being developed. The current breast phantom consists of a 3D-printed breast bucket filled with olive oil to simulate fatty tissue, and a tumour model. After contrast administration the tumour enhances, but so does the fibroglandular tissue, a process called background parenchyma enhancement (BPE). Therefore, the aim of this study is to increase the complexity of the breast perfusion phantom and develop a BPE phantom. Two fibroglandular tissue perfusion phantoms with perfusion capabilities, to simulate background parenchyma enhancement (BPE), were created based on the requirements set. The first BPE phantom is filled with sodium alginate beads, the second BPE phantom also contains a tumour with a diameter of 18mm. The phantoms were designed, 3D printed, and static 3D images and dynamic angiography images were made using the Siemens Artis Pheno C-arm. Time-intensity curves of five regions of interest (ROIs) in the BPE phantom with tumour were created from dynamic X-ray images. Particular focus was given to the comparison of the tumour ROI and the fibroglandular tissue ROIs. The time-intensity curves showed promising results, as the tumour ROI shows a significant higher intensity during enhancement than the fibroglandular tissue ROI, which is equivalent to the shape of the iodine concentration curves of a tumour and fibroglandular tissue in patients. The developed fibroglandular tissue perfusion phantoms can mimic background parenchymal enhancement and tumour perfusion and can be used as a tool for the validation of dynamic contrast-enhanced dedicated breast CT.

# Contents

<b>1</b>	<b>Introduction</b>	<b>1</b>
1.1	Screening modalities . . . . .	1
1.2	Dynamic contrast-enhanced breast computed tomography . . . . .	3
<b>2</b>	<b>Theoretical background</b>	<b>4</b>
2.1	Dynamic contrast-enhanced breast computed tomography . . . . .	4
2.2	Fibroglandular tissue . . . . .	4
2.2.1	Fibroglandular tissue distribution . . . . .	5
2.2.2	Fibroglandular tissue volume . . . . .	6
2.3	Background parenchymal enhancement . . . . .	6
2.4	Simulating microvascular blood flow . . . . .	6
2.4.1	Sodium alginate beads . . . . .	6
2.4.2	Gyroid structure . . . . .	6
<b>3</b>	<b>Requirements</b>	<b>7</b>
<b>4</b>	<b>Designs and fabrication</b>	<b>9</b>
4.1	Supplied SolidWorks parts . . . . .	9
4.2	Phantom volume . . . . .	9
4.3	Hemisphere phantom . . . . .	10
4.4	Loft phantom . . . . .	10
4.5	Gyroid phantom . . . . .	11
4.6	Fillable BPE phantom . . . . .	11
4.7	First fabrication . . . . .	12
4.7.1	Stereolithography printing . . . . .	12
4.7.2	Sodium alginate beads preparation . . . . .	12
4.7.3	New tube connectors . . . . .	13
4.7.4	Filling the phantom . . . . .	13
4.7.5	Glueing with epoxy . . . . .	14
4.8	New fillable BPE phantom . . . . .	14
4.9	BPE phantom with tumour . . . . .	15
4.10	Second fabrication . . . . .	16
4.10.1	Adjustments to the printed tumour tubing phantom . . . . .	16
4.10.2	New sodium alginate beads preparation . . . . .	17
4.10.3	Filling and glueing the phantoms . . . . .	17
<b>5</b>	<b>CT scans</b>	<b>18</b>
5.1	CT Set-up . . . . .	18
5.2	Fillable BPE phantom . . . . .	18
5.2.1	DCT head . . . . .	18
5.2.2	DSA . . . . .	19
5.3	BPE phantom with tumour . . . . .	20
5.3.1	DCT body . . . . .	20
5.3.2	FL angio . . . . .	20
<b>6</b>	<b>Results</b>	<b>22</b>
<b>7</b>	<b>Discussion</b>	<b>24</b>
<b>8</b>	<b>Conclusion</b>	<b>26</b>
<b>A</b>	<b>Appendix: Generative AI disclosure</b>	<b>30</b>

# 1 Introduction

Breast cancer is the most common form of cancer among Dutch women, about 1 out of 7 Dutch women will get breast cancer during her lifetime [1]. Worldwide, breast cancer is the most common form of cancer. With 2.3 million new breast cancer cases and 685,000 breast cancer deaths in 2020 worldwide, breast cancer is the leading cause of cancer death in females. [2] In the Netherlands, more than 3,000 women die of breast cancer every year [1].

## 1.1 Screening modalities

In order to detect this type of cancer, different screening imaging techniques can be used. For instance mammography, contrast-enhanced mammography (CEM), digital breast tomosynthesis (DBT) and dynamic contrast-enhanced magnetic resonance imaging.

### Mammography

In mammography, two views of each breast are acquired. To improve the image quality, the breast is compressed during imaging. Mammography involves a number of limitations, including the masking effect of the fibroglandular tissue, that may result in a decrease in the breast cancer detection rate [3]. When mammography is not sufficient to detect breast cancer, additional imaging is required during screening. Imaging techniques such as CEM and DBT can provide more information to detect breast cancer or other breast diseases. [4]

In x-ray breast imaging, contrast agent administration can enhance image quality and improve tumour visualisation. The contrast agent is selectively concentrated in the tumour after administration, due to tumour angiogenesis. By using the properties of tumour angiogenesis, contrast agents can overcome the lack of contrast between the tumour and fibroglandular tissue. Contrast enhancement increases lesion visibility, and when dynamic images are acquired, additional information on the kinetics of contrast uptake can be obtained. Therefore, more accurate diagnoses can be made. [5]

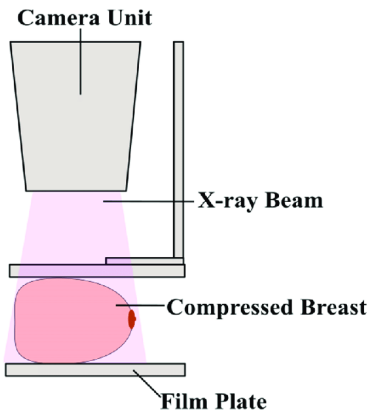


**Figure 1:** Mammography set-up for 2D acquisitions of the breast. [6]

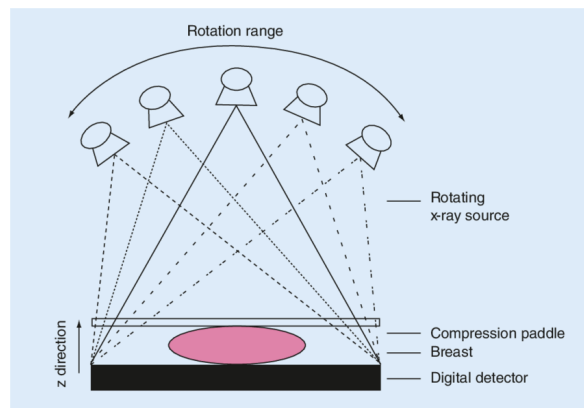


**Figure 2:** Digital breast tomosynthesis set-up for quasi 3D acquisitions of the breast with a rotating x-ray source. [7]

### Contrast-enhanced mammography

In contrast-enhanced mammography (CEM), standard mammography and administration of iodinated contrast agent are combined. In this technique, the areas of contrast uptake are made visible by using low-energy and high-energy images acquired in one acquisition using a dual-energy technique. These images are recombined and enable visualisation of the areas of contrast uptake. [8] The limitations of CEM include the radiation dose and the phenomenon of background parenchyma enhancement (BPE) that could mask possible lesions. BPE is the enhancement of the normal breast parenchyma by the administration of contrast. More about BPE can be found in chapter 2.3. [4]

### Digital breast tomosynthesis

Digital breast tomosynthesis (DBT), also called 3D mammography, is a quasi 3D x-ray imaging technique that can localise the depth of lesions and reduce the effect of tissue superposition [5, 9, 10]. The technique applies the same amount of pressure to the breast as in mammography, but instead of two images, DBT captures multiple images from different angles. Because the angle is limited, there is not enough information to reconstruct a full 3D volume; out-of-plane objects are blurred and the resolution in the planes parallel to the detector are significantly higher than the resolution in the perpendicular direction [11]. Compared to mammography, DBT has better visibility and specificity and offers better visualisation of the parenchyma structure [5, 9, 10]. Also, DBT can better define the stage of the disease than mammography. This is why this modality promises to be a sensitive method of detecting breast cancer, especially when used in combination with contrast agent [5].

### Dynamic contrast-enhanced magnetic resonance imaging

The imaging modality dynamic contrast-enhanced magnetic resonance imaging (DCE-MRI) is used for initial diagnosis and staging of tumours, as well as for the monitoring of response to chemotherapy or radiotherapy. It consists of fast MRI sequences obtained before, during and after the intravenous injection of a gadolinium contrast agent. This results in something comparable to a video in which gadolinium contrast agent can be followed over time, which can be used to assess tumour angiogenesis. [12]

Tumours can be distinguished from normal tissue in DCE-MRI because they show fast, intense enhancement during imaging, after which it is washed out relatively quickly compared to normal tissue [13]. Also, the tumour types can be distinguished based on the time-intensity curve (TIC), determined by the uptake and washout of contrast agent. A tumour is type 1 (persistent enhancement) if the signal intensity increases steadily in the TIC. A tumour is type 2 (plateau) if the peak intensity is reached early after contrast administration and this is followed by a signal intensity plateau in the TIC. A tumour is type 3 (washout) if the peak value in the TIC is reached early and the intensity then decreases. [14] A schematic representation of these time-intensity curves can be seen in figure 3.

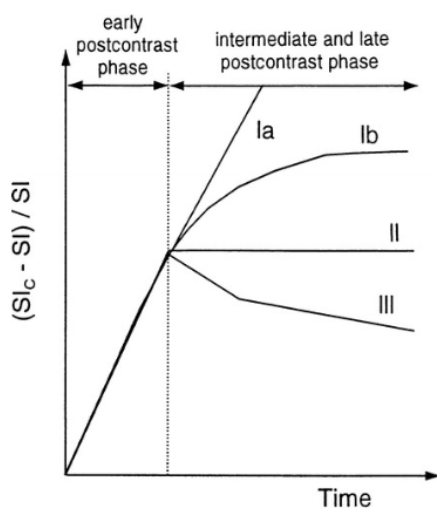


**Figure 3:** Schematic time-intensity curves of the three tumour types. Type I is a persistent enhancement curve with a straight (Ia) or curved (Ib) line, type II is a plateau curve and type III is a washout curve. The vertical axis is given by the formula for the wash-in rate, based on the relative signal intensity over time. [15]

Some disadvantages of MRI are that it has a longer acquisition time than CT. Also, MRI has limited availability depending on the area, and it is relatively expensive compared to other imaging modalities. [16]

## 1.2 Dynamic contrast-enhanced breast computed tomography

For diagnosis, treatment planning and response monitoring, a new imaging modality called dynamic contrast-enhanced dedicated breast computed tomography (DCE-bCT) is developed [3]. In this 3D imaging technique, an iodine contrast agent will be followed over time. The 3D imaging technique overcomes the masking effect of fibroglandular tissue, as present in mammography and DBT [17]. Furthermore, DCE-bCT has a limiting spatial resolution of 0.25 mm and temporal resolution of 5 seconds and, therefore, overcomes the limiting resolutions of DCE-MRI [18].

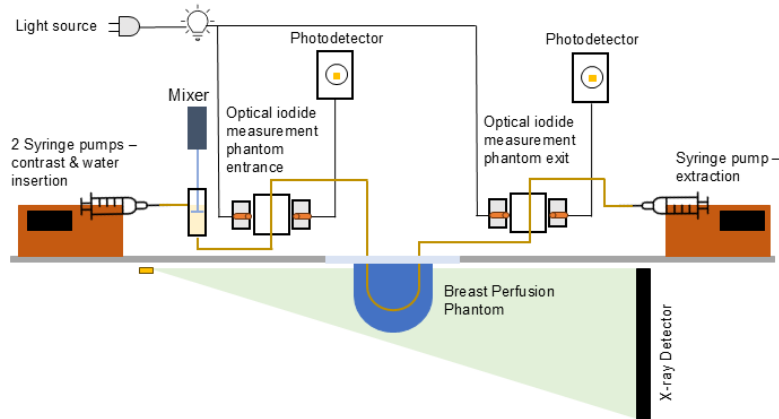


**Figure 4:** DCE-bCT set-up with a breast perfusion phantom with tubing and olive oil, an x-ray source and detector, two syringe pumps for water and contrast administration, an optical iodide measurement using a photodetector at the entrance and exit of the phantom and a syringe pump for extraction of the contrast and water. [19]

DCE-bCT still has to be validated and the acquisition and reconstruction parameters need to be optimized on a test object. So far, a simplified breast phantom has been developed for this purpose, as can be seen in figure 4. The phantom consists of a 3D printed breast bucket filled with olive oil to simulate fatty tissue, tubing, and the possibility of adding tumour phantom inserts [19]. However, the phantom lacks the simulation of fibroglandular tissue and its background parenchymal enhancement. Therefore, the aim of this project is to develop a fibroglandular tissue phantom enhanced with perfusion capabilities to simulate background parenchymal background enhancement (BPE) in breast CT. Also, a tumour phantom will be integrated to test the flow characteristics of BPE in combination with the tumour.

The research question of this project is: "How to develop a Fibroglandular Tissue perfusion Phantom, with background parenchymal enhancement, for the validation of dynamic contrast-enhanced dedicated breast CT?"

## 2 Theoretical background

In order to make an optimal fibroglandular tissue perfusion phantom, the location, size and shape of the fibroglandular tissue must be examined to represent the phantom as anatomically as possible. Also, more information about different ways of simulating blood flow should be collected, for example by using a gyroid infill pattern or sodium alginate beads. For more background information, dynamic contrast-enhanced dedicated breast CT and parenchymal background enhancement should be investigated. This associated literature research can be found in this chapter.

### 2.1 Dynamic contrast-enhanced breast computed tomography

What makes breast CT unique from traditional CT, is that the patient lies on the stomach and the detector rotates around one of the breasts lying on the table, as can be seen in figure 5. Also, the x-ray tube and the detector are optimized for breast tissue coverage and lesion detectability, this provides higher contrast and higher spatial resolution and allows for lower dose than traditional CT for breast imaging [17]. However, breast CT still provides limited information on tumour characteristics. To overcome this limitation, contrast-enhanced (CE) breast CT has been developed. Some studies have shown that CE breast CT has better enhancement of malignant lesions compared to normal breast CT [20] and that it also provides better specificity than CE breast MRI [21].

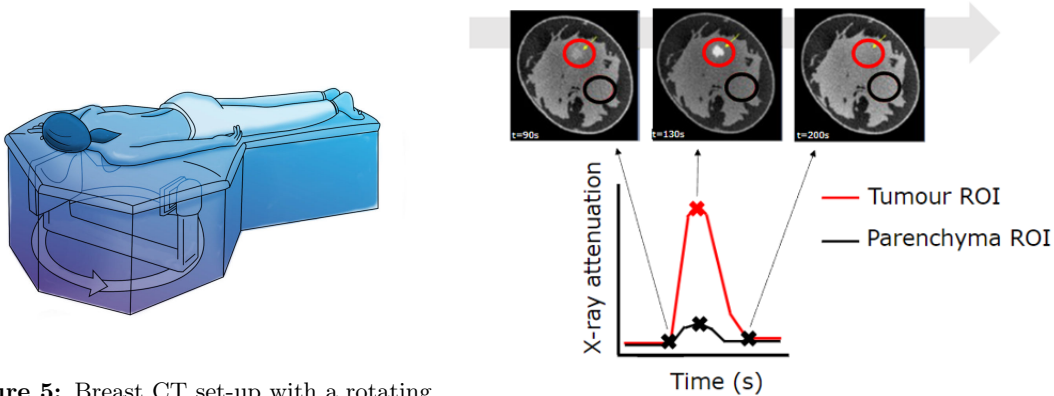


**Figure 5:** Breast CT set-up with a rotating x-ray source and detector. [22]

**Figure 6:** The difference in attenuation for the tumour ROI and the parenchyma ROI. [23]

Dynamic contrast-enhanced dedicated breast computed tomography (DCE-bCT) displays this contrast-enhanced information over time. This could be optimal for staging, treatment planning and treatment monitoring, since the temporality could provide valuable diagnostic and prognostic information [24]. When a DCE-bCT scan is performed, the visibility and details of the lesion morphology are enhanced and the functional behaviour can be characterized by examining the contrast uptake and outflow over time [17], as shown in figure 6. In this figure, the two regions of interest (ROI) are the parenchyma and the tumour. The tumour shows higher x-ray attenuation as a result of the contrast, since the tumour's vascularity is increased compared to 'normal' breast tissue. However, the parenchyma shows increased x-ray attenuation as well, due to background parenchymal enhancement.

### 2.2 Fibroglandular tissue

The fibroglandular tissue in the breast consists of two types of tissue. The fibrous connective tissue, also known as stroma, holds the tissue in place and the glandular epithelial cells, the parenchyma, cover the milk ducts in the breast and produce milk. Besides the fibrous connective tissue, the breast consists of fat. [25] Figure 7 shows how this is anatomically structured.

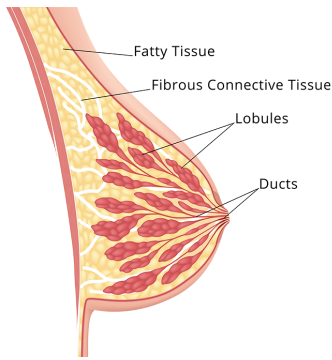


**Figure 7:** The breast anatomy with the fibroglandular tissue of the breast. [26]

Fat absorbs fewer x-rays than fibroglandular tissue. Therefore, fat areas appear darker on a breast x-ray image. Bright areas are associated with fibroglandular tissue. [25]

### 2.2.1 Fibroglandular tissue distribution

The distribution of fibroglandular tissue in the three-dimensional breast plays a major role in determining the breast dose for the patient. Therefore, Fedon et al., investigated the fibroglandular tissue distribution. As can be seen in figure 8, the fibroglandular tissue fraction in the breast is different for every direction. The fibroglandular tissue has a higher concentration in the anterior regions of the breast. Also, the middle part in x and y direction has a higher glandular fraction than the regions towards the sides of the breast. Regions close to the chest wall showed a low concentration of fibroglandular tissue. [27]

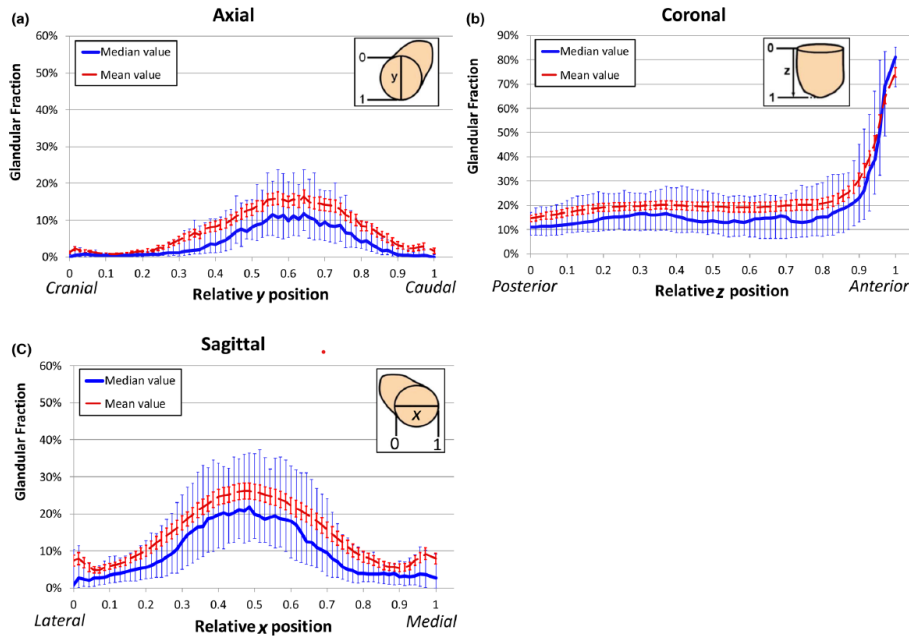


**Figure 8:** Distribution of glandular tissue fraction for (a) axial, (b) coronal and (c) sagittal view in the breast. The orientation of the breast can be seen in the inset. [27]

In another research done by Huang et al., also the distribution of fibroglandular tissue in a bCT image was determined. This research also showed that the fibroglandular tissue is mainly located near the breast nipple and in the centre part of the breast in three dimensions. [28]

### 2.2.2 Fibroglandular tissue volume

According to a study done by Vedantham et al., the average fibroglandular tissue percentage in the breast is equal to 14.95%. This is examined with digital breast tomosynthesis (DBT). [29]

The average fibroglandular tissue volume is also determined by using the research done by Fedon et al. By using the average glandular fraction of the relative x-, y- and z-positions (figure 8) the average fibroglandular tissue volume results in a percentage of 15.1% of the total breast volume. [27]

Therefore, approximately 15% of the total breast volume is formed by the fibroglandular tissue.

### 2.3 Background parenchymal enhancement

The breast parenchyma is part of the breast fibroglandular tissue and shows contrast enhancement when contrast agent is administered. This phenomenon is called background parenchymal enhancement (BPE) and can be seen in figure 6 by the enhancement of the parenchyma ROI. The enhancement depends on the venous circulation of the tissue and its permeability to the contrast agent [4]. Therefore, the enhanced images can reflect the blood circulation of the breast parenchyma and lesions [30]. Patients with dense breasts have significantly higher BPE [10].

### 2.4 Simulating microvascular blood flow

To mimic microvascular perfusion, sodium alginate beads or a 3D-printed gyroid structure can be used.

#### 2.4.1 Sodium alginate beads

Sodium alginate beads are beads formed by the chemical reaction between a sodium-alginate solution and a calcium lactate solution. Beads are formed when round drops of sodium alginate fall into the calcium solution. When alginate comes in contact with calcium, the alginate begins to cross-link. A gel shell is formed around the bead, which thickens as the beads remain in the solution, due to diffusion of calcium through the outer alginate gel layer. The alginate on the inside of the beads also begins to cross-link and forms a gel when it comes in contact with calcium. These resulting beads consist of 98% water. [31] An example of these beads can be seen in figure 9.

These beads can be used to simulate microcirculation blood flow by applying fluid flow. The fluid can move between these beads, mimicking the fine capillary network by small interconnecting tubes.



**Figure 9:** Sodium-Alginate beads, used to mimic the fine capillary network. [32]



**Figure 10:** A gyroid structure, used to simulate blood flow. [33]

#### 2.4.2 Gyroid structure

A 3D-printed gyroid structure can also be used to simulate microcirculation blood flow. In a gyroid structure, the fluid can flow in three dimensions, just like in the fine capillary network by small interconnected tubes. A picture of a gyroid structure can be seen in figure 10.

### 3 Requirements

To get a clear picture of the required functions and design of the fibroglandular tissue phantom, a list of requirements for the phantom was made. This list is divided into three groups, the phantom, functional and tumour requirements. The phantom requirements are those that ensure that the phantom mimics the fibroglandular tissue. The phantom requirements and their explanations can be found in table 1.

**Table 1:** Phantom requirements

Phantom requirement	Explanation
<b>I:</b> The location of the phantom must be based on the anatomical breast.	To place the phantom at the depth where most of the fibroglandular tissue is located in the anatomical breast.
<b>II:</b> The shape of the phantom must be based on the anatomical breast.	To mimic the shape of where most of the fibroglandular tissue is located in the anatomical breast.
<b>III:</b> The size of the phantom must be based on the anatomical breast.	In order to make the phantom as big as the average fibroglandular tissue volume in the anatomical breast, based on the average percentage of the total breast volume.
<b>IV:</b> The phantom should mimic perfusion of fibroglandular tissue.	To enable a flow inside the phantom that mimics the perfusion, the phantom should be fillable with Sodium-alginate beads or should be printed with a gyroid pattern on the inside.

The functional requirements are those that ensure that the phantom functions properly on dynamic CT scans. The functional requirements and their explanations can be found in table 2.

**Table 2:** Functional requirements

Functional requirement	Explanation
<b>I:</b> The phantom should be transparent.	To be able to see if the phantom contains any air bubbles. This can be done by printing the phantom with the stereolithography (SLA) 3D printer.
<b>II:</b> The phantom should be free of air bubbles.	To have no lowered image quality on CT images.
<b>III:</b> The phantom should have a wall thickness of 0.5 to 1 mm.	The wall should be strong enough to hold the filling without the phantom breaking, but the wall should not be too thick because of increased attenuation. This can also be done by using the SLA 3D printer.
<b>IV:</b> The phantom must contain 1 input and 1 output on the lid of the breast phantom, which can be connected to the tubing and the pump.	To allow fluid to flow through the phantom in one direction to make dynamic CT scans and mimic blood flow.
<b>V:</b> The phantom should be attached to the lid of the total breast phantom.	To make it possible to let the phantom 'float' in the breast phantom bucket.
<b>VI:</b> The phantom must be completely closed and watertight.	To prevent leakage of contrast and water outside the phantom into the breast phantom. This can also be done by printing with the SLA 3D printer and by using epoxy.
<b>VII:</b> The phantom must fit into a rounded cylinder with a maximum diameter of 119 mm and a maximum depth of 115 mm.	The phantom must fit into the total breast phantom bucket, which can be seen in figure 12, to allow complete closure of the entire breast phantom.

The tumour requirements are those that ensure that a tumour can be inserted into the phantom. The requirements and their explanation can be found in table 3.

**Table 3:** Tumour requirements

<b>Tumour requirement</b>	<b>Explanation</b>
<b>I:</b> The tumour has to fit inside the fibroglandular tissue phantom.	To make sure the tumour can be added to the developed phantom.
<b>II:</b> The tumour designs from S. Gouma's study [34] should be used.	The tumour designs are made specifically for this fibroglandular tissue phantom and are available.
<b>III:</b> About 80% of the contrast flow should go to the tumour phantom and 20% to the fibroglandular tissue.	To mimic the contrast distribution and flow as it is in the anatomical breast, this can be done by using a tubing with holes.

With these requirements, different designs are made and tested.

## 4 Designs and fabrication

This section contains all different fibroglandular tissue phantom designs that were created using SolidWorks and the fabrication of these phantoms.

### 4.1 Supplied SolidWorks parts

Before starting the design process, the supplied designs of the breast bucket and the lid have to be considered. The lid has a diameter of 117.50 mm and the tube connectors for addition of the flexible tubing are each positioned 30 mm from the centre of the lid. The breast bucket has a total height of 125 mm, the upper edge forms 10 mm of this. The indentations inside the upper edge are 5 mm. The breast bucket has an inner diameter of 119 mm and the wall thickness is equal to 1.5 mm. The shape and dimensions of the breast bucket and lid can also be found in figures 11 to 14.

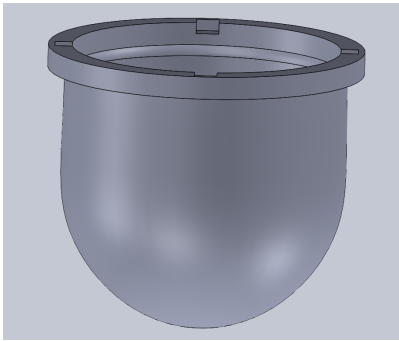


**Figure 11:** Breast bucket in front view.

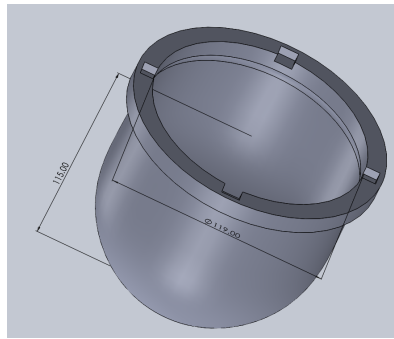


**Figure 12:** Breast bucket in front view with dimensions.

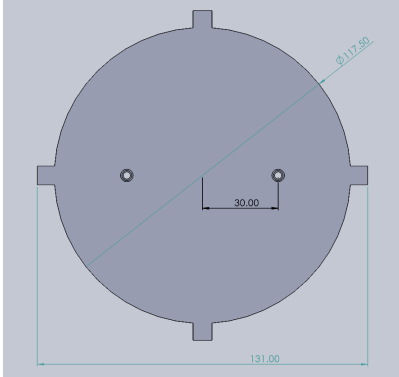


**Figure 13:** Lid of the breast bucket in top view with dimensions.

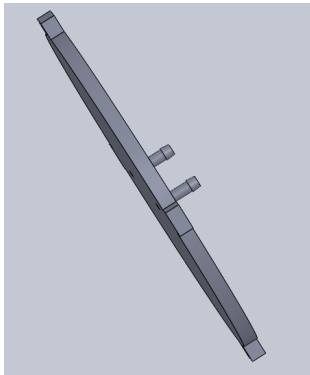


**Figure 14:** Lid of the breast bucket in front view.

### 4.2 Phantom volume

To determine the required volume of the fibroglandular tissue phantom, the total volume of the breast bucket should be determined. According to SolidWorks, the volume of the breast bucket is equal to  $V_{bb} = 1,138,019.90 \text{ mm}^3$ . The average fibroglandular tissue volume in the anatomical breast, as stated in chapter 2.2.2, is equal to approximately 15% of the total breast volume. Therefore, the fibroglandular tissue volume needs to be approximately equal to  $V_{ft} = 170,000 \text{ mm}^3$ .

### 4.3 Hemisphere phantom

For the first fibroglandular tissue phantom, the hemisphere phantom, some assumptions were made. The phantom meets all phantom and functional requirements except for phantom requirement I, II and IV. Whether functional requirement II is met is uncertain until fabrication. Phantom requirement III is met because the phantom should have a volume of approximately  $170,000 \text{ mm}^3$ . The shape of this phantom is a hemisphere, attached to the lid of the breast bucket. The radius of the hemisphere could be determined using the following formula for calculating the volume of a hemisphere:

$$V = \frac{1}{2} \cdot \frac{4}{3} \pi r^3 \quad (1)$$

Reorganising this formula results in:

$$r = \sqrt[3]{\frac{3V}{2\pi}} \quad (2)$$

What results in:

$$r = 43,30 \text{ mm}$$

With this specific radius, a hemisphere phantom was made. The first hemisphere SolidWorks assembly was then constructed with the hemisphere phantom, lid and breast bucket. This can be seen in figure 15.

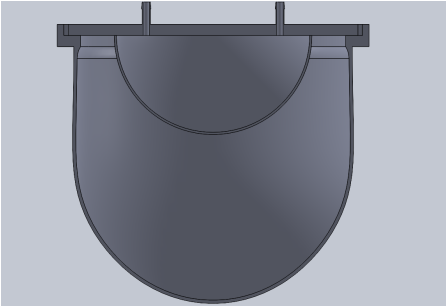


**Figure 15:** Hemisphere phantom assembly in front view.

### 4.4 Loft phantom

The loft phantom meets more requirements than the hemisphere phantom. Phantom requirement I and II were also met, because the shape and location of the phantom are based on the anatomical breast, as discussed in chapters 2.2.1 and 2.2.2. All the other requirements that were already met in the hemisphere phantom were also met in this phantom. The phantom was made using the loft feature in SolidWorks. The volume  $V_{ft}$  is equal to  $168,669.57 \text{ mm}^3$ . The height of the phantom is equal to 113 mm, the width 92 mm and the depth 68 mm. The wall thickness is equal to 1 mm.

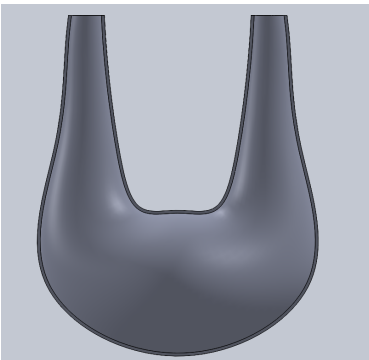


**Figure 16:** Loft phantom in front view.

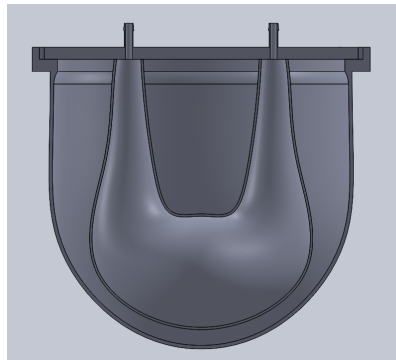


**Figure 17:** Half of the loft phantom assembly in front view.

Phantom requirement IV will be met when a gyroid structure is printed inside the phantom or when the phantom can be filled with sodium alginate beads.

#### 4.5 Gyroid phantom

To make the gyroid phantom, a gyroid structure and the loft phantom were combined. The inside of the loft phantom was filled with the gyroid to mimic the microvascular blood flow in the fibroglandular tissue. This results in the design that can be seen in figures 18 and 19.



**Figure 18:** Gyroid phantom in front view.

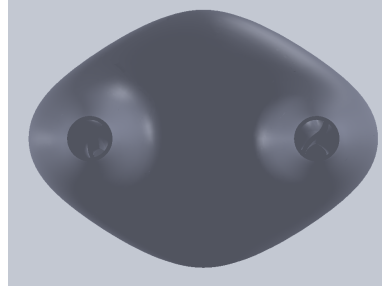


**Figure 19:** Gyroid phantom in top view.

Unfortunately, when the design was ready to be printed, it turned out that the gyroid structure in the phantom could not be printed using a resin printer. This was because there would be resin left inside the phantom when it was printed, causing it to deform. Also, the gyroid structure was not strong enough to make the whole phantom solid, so internal supports had to be added. However, the printed internal supports would no longer be accessible and could therefore not be removed. Since a fillable phantom, filled with sodium alginate beads and not a gyroid was more promising, it was decided not to print the gyroid phantom but to develop a fillable BPE phantom.

#### 4.6 Fillable BPE phantom

To make the loft phantom fillable, a cut line was introduced, making the phantom consist of two parts that can be glued together after filling. A lip and groove pattern was added to the cut line to ensure that the upper and lower parts of the phantom fit well together. The design of this phantom can be seen in figures 20 to 22. Functional requirement VI must be tested because the phantom may leak contrast and water if it consists of two parts that are not completely watertight when assembled. To ensure that the phantom does not leak, the two parts were glued together using epoxy.



**Figure 20:** Total fillable BPE phantom in front view.



**Figure 21:** Upper part fillable BPE phantom in front view.



**Figure 22:** Lower part fillable BPE phantom in front view.

## 4.7 First fabrication

This chapter shows the fabrication steps of the first printed phantom, the fillable BPE phantom. It involves several steps, such as stereolithography printing, preparing sodium alginate beads, making epoxy, gluing the phantom together and adding the tube connectors.

### 4.7.1 Stereolithography printing

The first step of fabrication was to load the SolidWorks design files in the PreForm 3D printing software to determine the optimal printing configuration and to generate the support needed to print the design. After this, the design could be printed using the FormLabs Form 3L printer with Clear V4 resin. When the print was finished, the print was removed from the building platform of the printer and the support removed from the printed parts. The parts were cleaned using isopropyl alcohol (IPA), in all these steps, wearing gloves is recommended. The parts were placed in the IPA bath for 10 minutes and after the IPA bath, the parts were blow-dried with an air gun. To make sure all the resin was removed, the parts were placed a second time in the IPA bath for about five minutes and blow-dried again. The building platform was also cleaned with IPA. These steps were done to remove the uncured resin, before the resin was hardened in the oven. After all the resin was removed, the prints were placed in the FormLabs Form Cure L for 15 minutes with a temperature of 60 °C, as can be seen in figure 23.

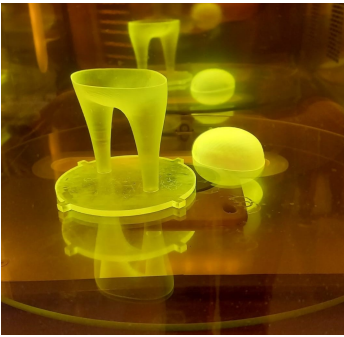


**Figure 23:** Fillable BPE phantom curing in the FormLabs Form Cure L.

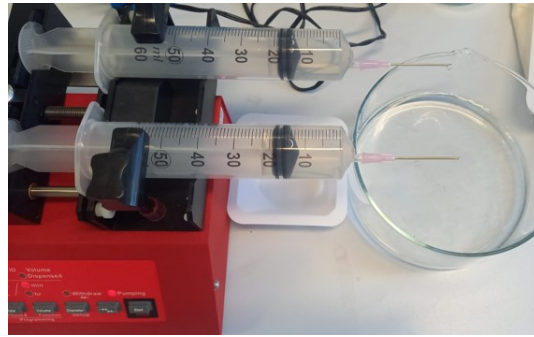


**Figure 24:** Sodium alginate beads preparation with a syringe pump and two syringes with injection tips.

### 4.7.2 Sodium alginate beads preparation

The preparation of sodium alginate beads was done in the lab. This chapter describes the materials and steps needed to form enough beads for one phantom. Figure 24 shows a part of the set-up used to prepare the beads. Using this method, the diameter of the beads will be approximately 3 mm.

#### Materials

- 6 grams of sodium alginate powder (Special Ingredients Europe)
- 10 grams of calcium lactate powder (Special Ingredients Europe)
- 2 high beakers of at least 300 mL
- Laboratory bottle
- 700 mL of Milli-Q Type 1 (Ultrapure)
- Magnetic stirrer with magnets
- Syringe pump
- 2 syringes of at least 60 mL
- 2 injection syringe tips
- 1 low beaker with a minimum radius of 7 cm
- Fridge
- Colander
- Funnel

## Methods

1. Add 300 mL of Milli-Q to a high beaker and place it on the magnetic stirrer, with a clean stirring magnet inside the beaker. Let the magnet spin on a medium speed.
2. Add 6 grams of sodium alginate to this Milli-Q beaker. Completely dissolve the sodium alginate with the magnetic stirrer on a speed of 750 up to 900 rounds per minute, when needed increase or decrease the speed. The solution can become very viscous and must be mixed until all clumps are gone, this takes approximately one hour. To make the solution air bubble free, it may be useful to leave the solution in the fridge for a minimum of eight hours.
3. Meanwhile, add 200 mL of Milli-Q to a high beaker and place it on the magnetic stirrer, with a clean stirring magnet inside the beaker. Let the magnet spin at a speed of 750 up to 900 rounds per minute.
4. Add 10 grams of calcium lactate to this Milli-Q beaker. Completely dissolve the calcium lactate with the magnetic stirrer. Keep stirring until all calcium lactate clumps are completely dissolved. This takes approximately thirty minutes.
5. The following steps can be performed if both solutions are completely air bubble free. Fill a large, low beaker to half its maximum volume with the 5% calcium lactate solution.
6. Fill the 2 syringes with the 2% sodium alginate solution and add the syringes to the syringe pump. Add the injection tips to the syringes with the open part pointing down.
7. Place the syringe injection tips over the beaker at 5 cm above the calcium lactate and turn on the syringe pump at a speed of 1.50 mL/min. At this speed, a total of 3 mL of sodium alginate per minute will fall into the calcium lactate solution, forming the sodium alginate beads.
8. Once the low beaker is almost filled with sodium alginate beads, turn off the syringe pump and remove the beads from the solution by using a colander. Add them to a laboratory bottle with 200 mL of Milli-Q, using a funnel can be useful here. Place the low beaker again under the syringe tips and turn on the syringe pump. Add more calcium lactate solution to the low beaker when the volume becomes less than half the volume of the beaker.
9. Repeat steps 6 to 8 until there is no sodium alginate solution left or the syringes are empty. When more beads are needed, start again at step 1.
10. Store the beads in a laboratory bottle with all the beads below the Milli-Q surface and place it in the fridge until use.

### 4.7.3 New tube connectors

Unfortunately, after printing and curing, the tube connectors on the lid of the phantom were still soft and broke off. Therefore, new tube connectors had to be added to the phantom. To do this, the places where the tube connectors were attached were hollowed out with a column drill, the diameter of the drill bit was 5 mm. Using these holes, the last sodium alginate beads could be added to the phantom to fill it completely. The new tube connectors were small white plastic tube connectors, with nearly the same size as the original connectors. They were glued into this hole after the phantom was filled with the sodium alginate beads, as can be read in the following chapters.

### 4.7.4 Filling the phantom

To fill the phantom with sodium alginate beads, the phantom was rotated such that the upper part with the 'legs' would contain most of the beads. After it was filled, the lower phantom part was glued to the filled part with epoxy, which can be read in chapter 4.7.5. After the glueing, the phantom was completely filled through the hollowed-out holes of the connectors. To prevent the beads from drying out, tap water was added to the phantom.

#### 4.7.5 Glueing with epoxy

In order to glue the two parts of the phantom together and to add the new tube connectors to the phantom, epoxy casting resin UV was used. The epoxy resin and epoxy hardener were added to the mixing cup in a 1:1 ratio, 5 grams of both, and mixed very well with a stirring stick for three minutes. To make the epoxy more viscous and harden a little, let it stand for a sixty to ninety minutes. Check if it is ready to use by stirring the epoxy. After this, the epoxy was carefully attached to the parts with a syringe. After all parts were glued together, the epoxy was cured for 24 to 48 hours in the fridge. Before and after use, the beads were also kept in the fridge to ensure the beads have a longer durability. Figure 25 shows what the phantom eventually looked like.



**Figure 25:** Completely fabricated fillable BPE phantom.

#### 4.8 New fillable BPE phantom

As could be read in the previous chapters, a few difficulties were encountered in the fillable BPE phantom. Therefore, improvements were made in a new design.

The lip and groove pattern on the cutting line was not necessary because it was a very narrow pattern, due to the very low wall thickness. This did not make a difference in making the phantom waterproof, since the epoxy by itself already made the phantom waterproof. It was therefore chosen to leave out the pattern in the new design.

The cutting line, which divides the phantom into two pieces, has been moved upwards, to 81 mm from the top of the lid. At this height, the line creates the largest open space needed to place a tumour phantom inside the phantom in the next stage.

The tube connectors are reinforced to make sure they will not break off again. To do this, the wall thickness has been increased to 0.5 mm. The inner diameter of the tube connectors is now 2.80 mm and the largest outer diameter 5.00 mm. This made the connectors wider, but not too wide, to make sure the flexible tube still fits around them.

Since it is difficult to completely fill the phantom, an additional cutting line has been inserted into the bottom of the phantom. This extra cutting line makes it possible to fill the phantom through a hole with a diameter of 8 mm. When the phantom is fully filled, a small 'cap' can be glued into this hole with epoxy, to close the phantom completely. The new fillable BPE phantom is therefore composed of three parts, the lid containing the upper part of the phantom, the lower part of the phantom and the cap. This whole phantom can be seen in figures 26 and 27.

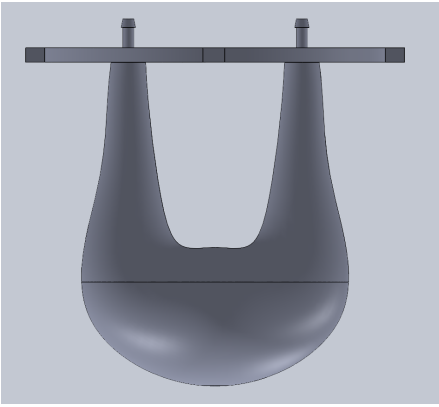


**Figure 26:** New fillable BPE phantom in front view.

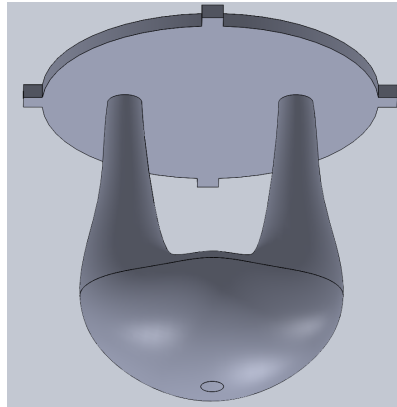


**Figure 27:** Total fillable BPE phantom.

#### 4.9 BPE phantom with tumour

The BPE phantom with tumour is in general the same as the new fillable BPE phantom, besides that this phantom contains a tumour part with additional tubing towards the tumour. This tumour has a diameter of 18 mm and contains a gyroid pattern with gyroid holes with a diameter of 1.5 mm [34]. The tumour tubing has an outer diameter of 4 mm and an inner diameter of 2.20 mm. The tube connectors have an inner diameter of 2.80 mm and the biggest outer diameter is 5.00 mm. The tube connectors are part of the tumour tubing part instead of the lid. The lid contains 2 holes with a diameter of 5 mm, in order to insert the tumour tubing connectors through these holes to connect the tubes. In this way, the total phantom can be constructed from four parts, the lid with upper part of the phantom, the lower part of the phantom, the small cap and the tumour tubing with tube connectors.

The tumour tubing contains fourteen small holes in each tube, distributed over four perpendicular sides, to make sure that water and contrast is able to move out and into the tumour tubing. As can be seen in figure 6, the tumour ROI shows more enhancement than the parenchyma ROI. This effect is mimicked by the holes in the tubes, since it is assumed that through these holes a bit of contrast and water is able to move out of the tubing into the fibroglandular tissue, but that most of the contrast and water stays in the tubing that leads to the tumour. The holes have a diameter of 0.80 mm, based on a printing experiment. In this experiment a thin rectangular plate with holes with a diameter of 0.05, 0.1, 0.2, 0.3 up to 2.3 mm has been printed. The purpose of this experiment was to determine the real accuracy of the resin 3D printer. The smallest printed hole which was completely open was the one with a diameter of 0.8 mm, as can be seen in figure 28 in the right upper corner. Therefore, this diameter has been used for the tumour tubing holes. The designs of the BPE phantom with tumour can be seen in figures 29 to 31.

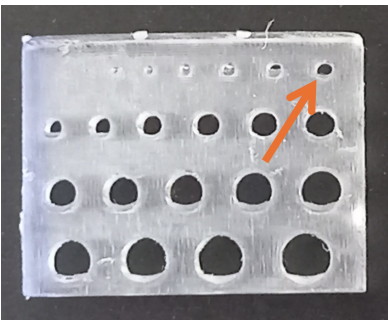


**Figure 28:** Test plate of the holes' accuracy, with in the right upper corner the hole with a diameter of 0.8 mm.

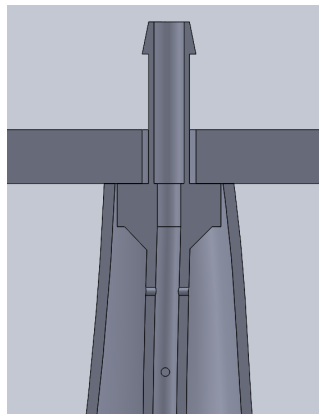


**Figure 29:** BPE phantom with tumour tubing close-up in front view.

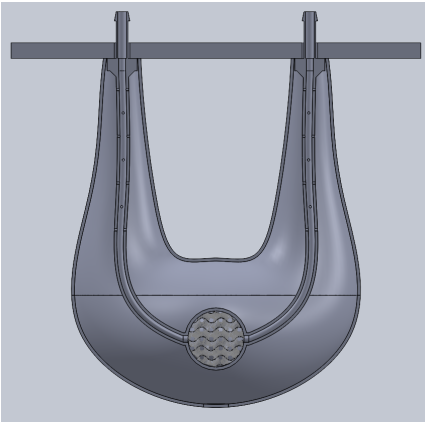


**Figure 30:** Total BPE phantom with tumour in front view.

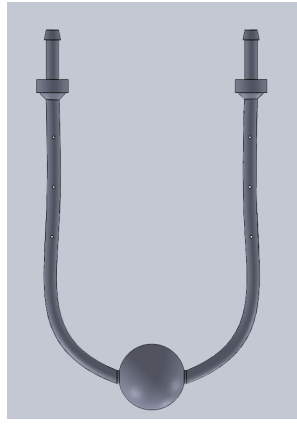


**Figure 31:** Tumour tubing for the BPE phantom with tumour in front view.

## 4.10 Second fabrication

During the second fabrication, the new fillable BPE phantom with modifications and the BPE phantom with tumour were printed in the same way as described in chapter 4.7.1. Figure 32 shows the parts of the BPE phantom with tumour and the new fillable BPE phantom curing in the FormLabs Form Cure L. Figure 33 shows the 3D printed tumour tubing.



**Figure 32:** New fillable BPE phantom and BPE phantom with tumour curing in the FormLabs Form Cure L.



**Figure 33:** 3D printed tumour tubing.

### 4.10.1 Adjustments to the printed tumour tubing phantom

Once the BPE phantom with tumour was printed, the tumour tubing part was tested on flow dynamics. With flexible tubing and a syringe, the tumour tubing was flushed with IPA to clean the inside of the tubing and the tumour. It was observed that most of the IPA flushed out of the tubing through the holes and that not much IPA reached the tumour, although the intention was for most of the fluid to reach the tumour and only some fluid to leave the tubing through the holes. Therefore, the number of holes are reduced to four holes on the side where the liquid enters the total phantom and eight holes on the side where the liquid leaves the total phantom.

It also became clear that the tumour tube connectors did not fit through the holes in the lid, so the tumour tubing SolidWorks part was modified with narrower tube connectors, with an outer diameter of 4.2 mm instead of 5.0 mm.

The cap for the bottom of the phantom was also too large to fit in the hole provided, so this part was modified. The diameter became 7 mm instead of 8 mm. However, after the new small cap was printed, it became clear that the cap was now too small instead of too large to fit into the designated

hole. Therefore, it should be best to make the small cap with a diameter of 7.5 mm. To properly close the already printed phantom, the 8 mm diameter cap was glued on top of the designated hole.

#### 4.10.2 New sodium alginate beads preparation

The preparation of the sodium alginate beads for both new phantoms was done as described by the methods of chapter 4.7.2. Because this time two phantoms must be filled with sodium alginate beads, the amount of sodium alginate solution and calcium lactate solution was doubled. Therefore, 1400 mL Milli-Q, 12 grams of sodium alginate powder and 20 grams of calcium lactate powder were used. Also, the high beakers must have a minimum capacity of 600 mL instead of 300 mL. Except for the doubled quantity, the preparation was done the same as in chapter 4.7.2.

After preparing the BPE phantom with tumour, the total weight of the beads in this phantom was determined, what was equal to 114 grams. Because the fillable BPE phantom has a larger free volume, the weight of the beads in this phantom was more than 114 grams.

#### 4.10.3 Filling and glueing the phantoms

To fill the BPE phantom with tumour with sodium alginate beads, the lid of the phantom was placed with the 'legs' pointing upwards on a beaker. The tumour tubing was added to this upper part of the phantom, with the tube connectors inserted through the holes of the lid. After this, the 'legs' of the phantom were filled with sodium alginate beads. To ensure that the phantom is filled as quickly as possible, it is best to form a pile of beads on the upper part and the tumour. After this, the large cap can be placed over this pile and these two parts can be glued together with epoxy. Make sure the epoxy is ready to use, as can be read in chapter 4.7.5. Once the two parts are glued together, the next step is to fill the phantom through the small hole in the large cap, using a funnel can be very useful here. With a small stick, the beads can be spread well over the phantom, without leaving empty spaces. When the phantom is fully filled, the small cap can be glued onto the phantom to make the phantom watertight. When using the epoxy, it may be useful to apply two layers and to cover all the gaps completely, to make the phantom completely watertight.

During the fabrication of this phantom, the tube connectors were glued to the lid after the phantom was completely filled. This was done using acryfix and making a circle of acryfix around the tube connectors on the lid to make the phantom properly watertight. Then the UV lamp was shone on the glued part to let the acryfix cure. It is recommended to glue the parts together with epoxy before filling the phantom, as epoxy can then also be applied between the lid and the blocks on the tumour tubing, ensuring that these parts are firmly attached to each other and that the phantom is completely watertight.

The result of the BPE phantom with tumour can be seen in figures 34 and 35.



**Figure 34:** Fabricated BPE phantom with tumour in front view.

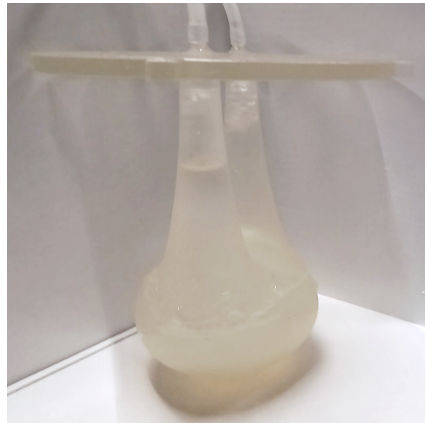


**Figure 35:** Fabricated BPE phantom with tumour in side view.

## 5 CT scans

### 5.1 CT Set-up

To be able to generate cone beam CT (CBCT) and angiography images of the phantoms, the set-up as in figure 36 was used. This set-up consists of the Siemens Artis Pheno C-arm, in which different imaging protocols were used. All phantoms were first scanned statically in 3D, and then dynamic images were made using the angiography acquisition protocol. The relevant phantom was placed in a container filled with water for minimal contrast of the environment, and the flexible tubes were attached to the phantom to make fluid flow possible using the pump. The pump has one input and one output. The input is connected to the water reservoir and the output is connected to a three-way valve, which is connected to an additional contrast pump and the phantom. The output leads the water and the contrast through the phantom to an output reservoir. The iodine contrast agent used is Iomeron 400, which contains 400 mg of molecular iodine per ml.

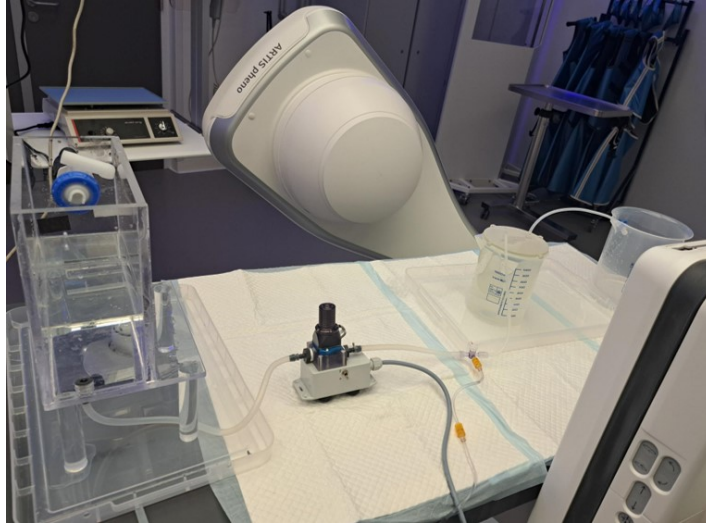


Figure 36: Set-up for CT images using the Siemens Artis Pheno CT.

### 5.2 Fillable BPE phantom

This chapter shows the different imaging protocols used to image the fillable BPE phantom and the resulting images of this experiment. During the protocols, images are made with and without iodine contrast agent.

#### 5.2.1 DCT head

To make sure there is no reduced image quality during the CBCT and angiography imaging experiments, the phantom should be free of air bubbles. To achieve this, the phantom was placed on a laboratory platform shaker and moved up and down by hand to tap the air bubbles out of the phantom. Using the protocol '6s DCT head' with a kilovoltage peak of 70 kVp, a full 3D scan of the phantom was made, to be able to see if the phantom contains air bubbles or other abnormalities. This scan resulted in 369 slices, some of which are shown in figures 37 up to 39. Unfortunately, this method did not remove all air bubbles, as a few air bubbles remained in the 'legs' of the phantom. These air bubbles are indicated with arrows in figures 37 and 39. For this experiment, it was decided that keeping these small air bubbles was not a problem, as the effect of the air bubbles on the flow simulation and image quality was considered negligible.

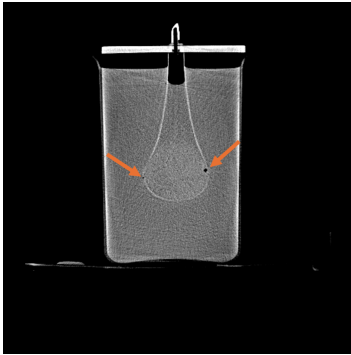


**Figure 37:** The 'legs' of the phantom with air bubbles indicated with arrows.

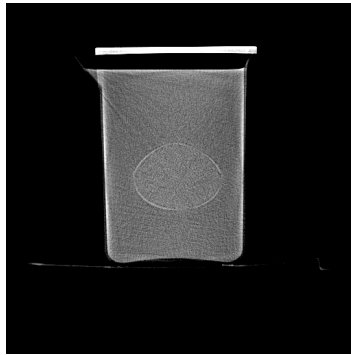


**Figure 38:** The 'belly' of the phantom without air bubbles.

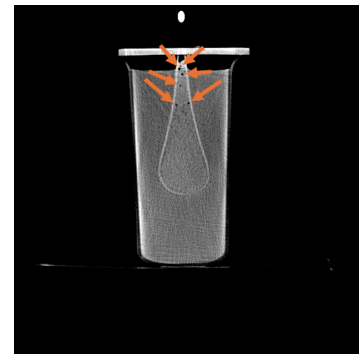


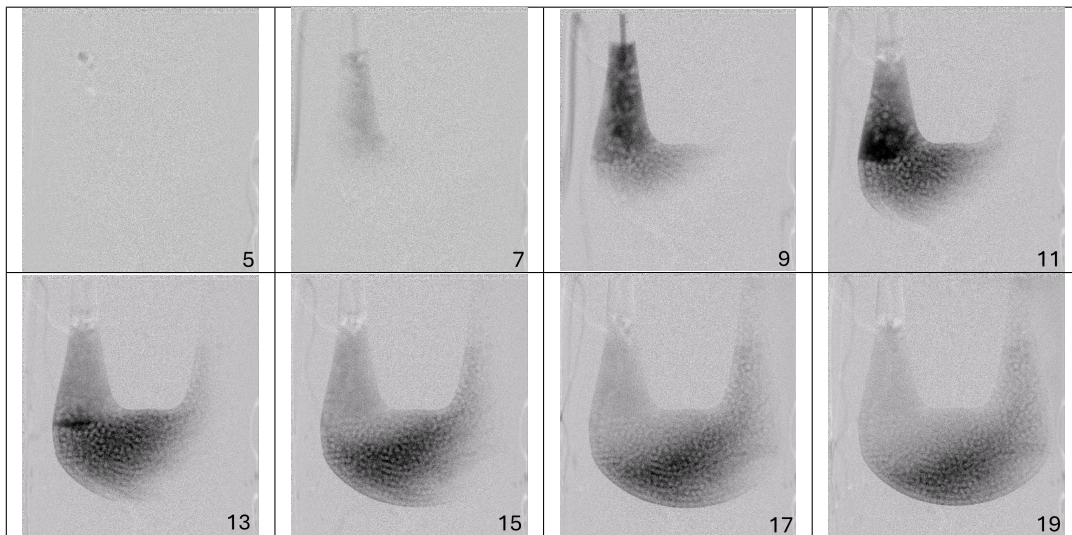
**Figure 39:** The 'legs' of the phantom with air bubbles indicated with arrows.

### 5.2.2 DSA

Using the 'Digital Subtraction Angiography (DSA) Care 2' protocol, dynamic x-ray images of the administration of contrast were made. During this scan, the pump allowed water and contrast to flow through the phantom. In a DSA, the CT scanner is used as an x-ray scanner, since 2D projections are made of 3D objects. In a DSA the first image is subtracted from all other images made, therefore only the changes with respect to the first image are visible.

For the DSA images with contrast, first, water is flowing through the phantom for approximately six seconds, after which 4 mL of (400 mg I/mL) iodine contrast agent is administered during 4 seconds, this results in a contrast flow of 1 ml per second. In table 4, the DSA images of this contrast administration are shown. After the contrast administration water is again flowing through the phantom. The frame rate was equal to 2 frames per second (fps), so the flow in table 4 took place in fourteen seconds. In the frames can be seen that the contrast spreads over the phantom and flows to the bottom right corner of the phantom, from where it slowly flushes out.

**Table 4:** DSA images are shown from the 5th to the 19th second, as indicated by the number in the bottom right corner of each image.



### 5.3 BPE phantom with tumour

This chapter shows the different imaging protocols used to image the BPE phantom with tumour, with and without using iodine contrast agent. It also shows the resulting images from this experiment. During this experiment, the same set-up as in the previous experiment was used, as described in chapter 5.1. This set-up can be seen in figure 36. The flow of the pump in this set-up is equal to 3.1 ml per second.

#### 5.3.1 DCT body

As also described in chapter 5.2, the phantom should be free of air bubbles to make sure there is no reduced image quality during the CT imaging experiment. To achieve this, the BPE phantom with tumour was moved up and down by hand and tapped against a beaker to tap the air bubbles out of the phantom. Using the protocol 'DCT body' with a kilovoltage peak of 90 kVp, a full 3D scan of the phantom was made, to be able to check if the phantom contains air bubbles or other abnormalities. This scan resulted in 376 slices, some of them are shown in figures 40 and 41. In these figures can be seen that this method did not remove all air bubbles, the air bubbles are indicated with arrows. For this experiment, it was also decided that keeping these small air bubbles was not a problem, as the effect of the air bubbles on the flow simulation and image quality was again considered negligible.

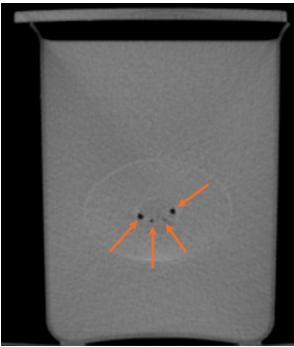


**Figure 40:** The tumour with air bubbles indicated with arrows.

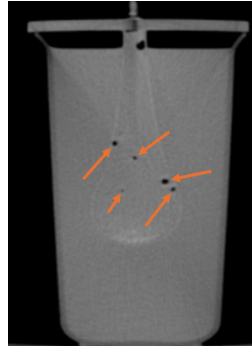


**Figure 41:** The 'legs' of the phantom with air bubbles indicated with arrows.

#### 5.3.2 FL angio

The 'fluorescein angiography imaging protocol (FL angio)' was used to image the BPE phantom with tumour with iodine contrast agent. With this protocol, dynamic and static x-ray images were taken. The dynamic x-ray images were taken from the administration of contrast. The static x-ray images were taken to check from one to seven minutes after the start of the dynamic images whether the contrast agent had already been flushed out of the phantom. The pump allowed water and contrast to flow through the phantom during both scans.

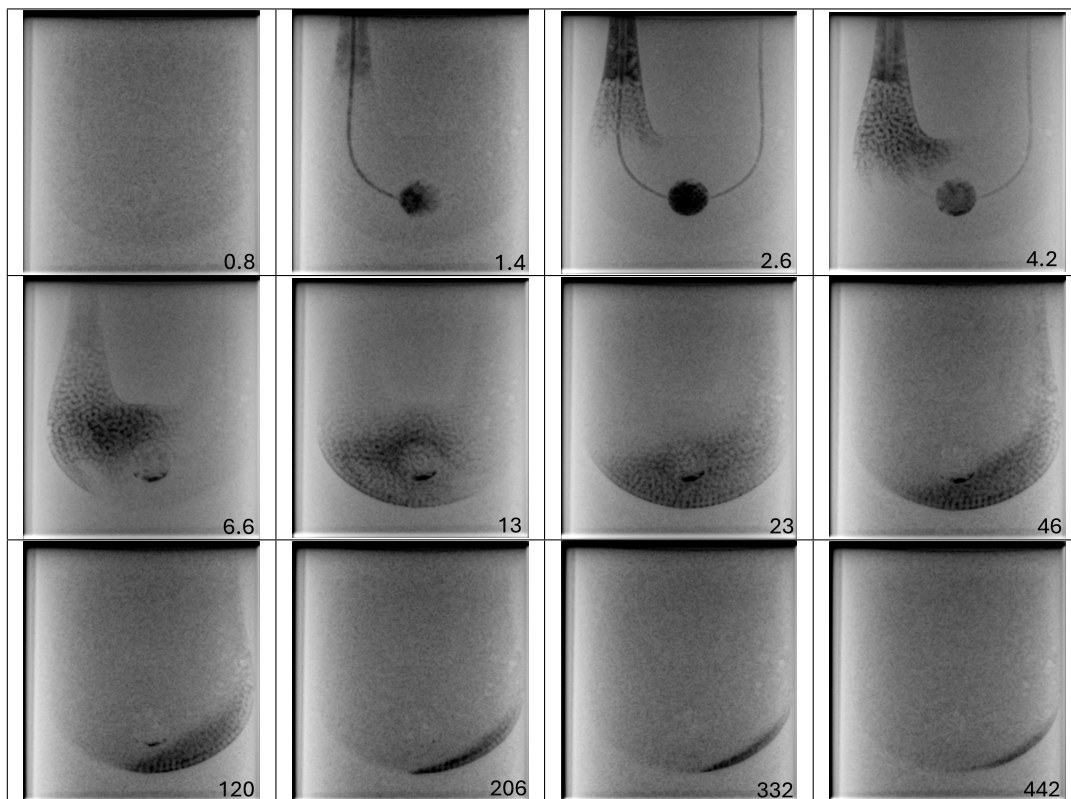
##### Dynamic images

For the dynamic image sequence with contrast, first water flows through the phantom for about a second, then 4 ml of (400 mg I/mL) iodine contrast medium is administered for 4 seconds, resulting in a contrast flow of 1 ml per second. After this, water flows through the phantom again. The first two rows of table 5 show the images of this dynamic imaging sequence, which lasted 46 seconds. The frame rate was equal to 5 fps.

##### Static images

The last row of table 5 shows the static FL angio images taken after the dynamic image sequence to check whether the added contrast was flushed out of the phantom.

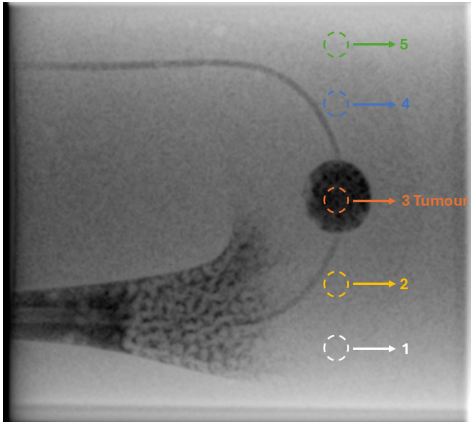
**Table 5:** The dynamic FL angio images taken at 0.8 to 46 seconds and the static FL angio slices taken at 120 to 442 seconds after the start of the dynamic image sequence, as indicated by the number in the right bottom corner of each image.



In the frames of table 5 it can be seen that the contrast enters the tumour tubing and the tumour and that the contrast is able to leave the tumour tubing, from where it distributes over the phantom. The contrast flows to the bottom of the tumour and the bottom right corner of the phantom, from where it slowly flushes out.

## 6 Results

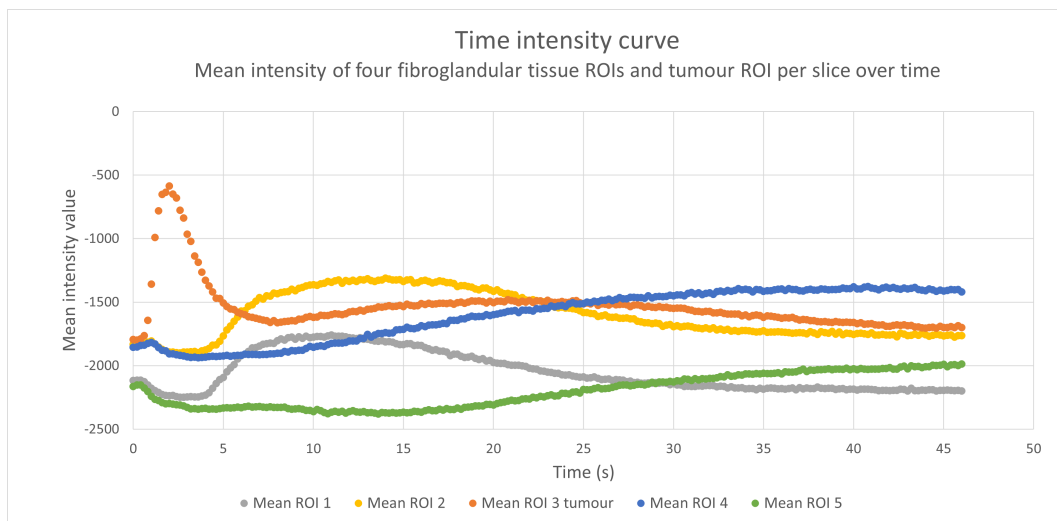
From the dynamic and static x-ray images of chapter 5.3.2, five ‘Regions of Interest’ (ROIs) are selected, their location can be seen in figure 42.



**Figure 42:** The regions of interest of the FL angio images. The colours correspond to the colours of the time-intensity curves.

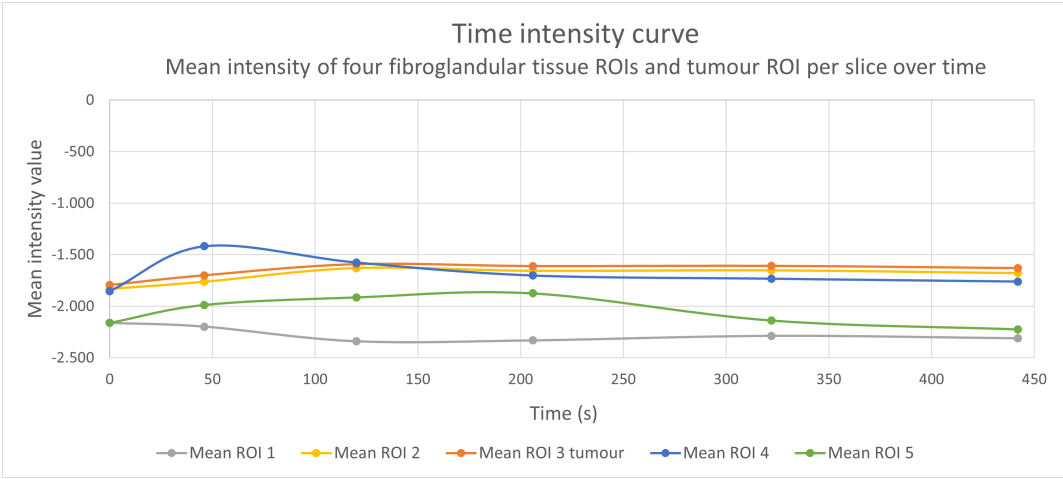
Of these ROIs, the mean intensity values per ROI over time are determined using the ImageJ image processing program. These values are plotted as a function of time to create time-intensity curves, this allows the intensity values of the different ROIs to be compared. A higher concentration of contrast agent results in a higher attenuation of x-ray beams and a lower mean intensity value. The mean intensity values are multiplied by minus one to make reading the graphs more intuitive, as the intensity value peaks when a higher concentration of contrast agent reaches an ROI. Using these time-intensity curves, it becomes clear how the contrast spreads over the phantom.

In figures 43, 44 and 45 the time-intensity curves of the dynamic and static images can be seen. Every ROI shows a different starting mean intensity value since every ROI is made of a 2D projection of the 3D phantom and the phantom does not have a uniform thickness. Therefore, it can be seen that ROI 1 and 5 have a higher mean intensity value because fewer x-rays are attenuated given that the phantom is smaller there. When comparing the curves, it is important to consider the different starting intensities and the thickness of the phantom.



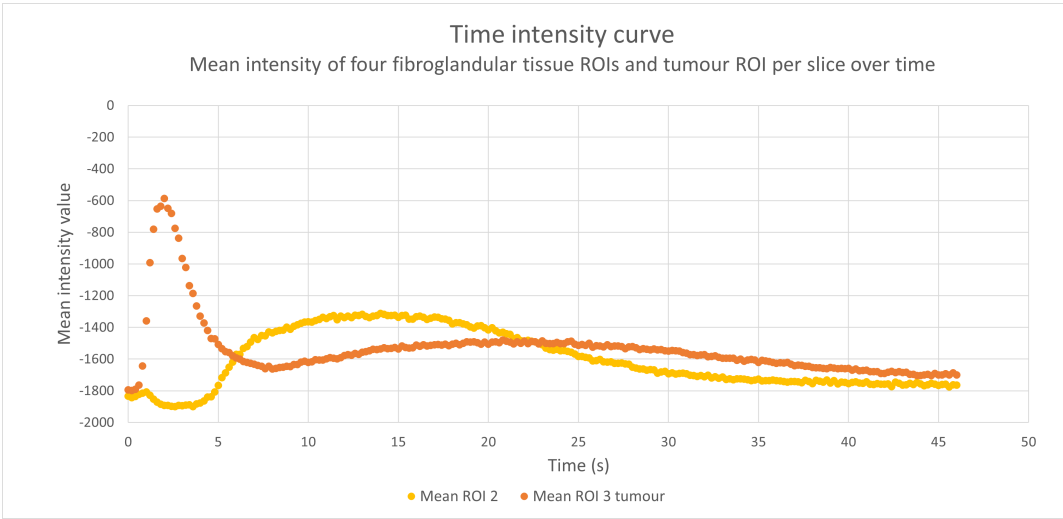
**Figure 43:** Time-intensity curves of the four fibroglandular tissue ROIs and one tumour ROI of the dynamic x-ray images.

Figure 43 shows the time-intensity curves of the four fibroglandular tissue ROIs 1, 2, 4 and 5, and the tumour ROI 3. These curves are made of the dynamic x-ray images of five fps during contrast administration. Figure 44 shows the time-intensity curves of the same ROIs, but in this graph the first and last dynamic x-ray images and all static x-ray images are plotted. The static x-ray images were taken after the dynamic x-ray images, to monitor whether the contrast flushes out of the phantom and tumour. In this graph, the flow of contrast can be followed over a longer time. It can be seen that the mean intensity value at the end of the curve nearly reaches the same value as at the start of the curve, showing that nearly all contrast left the phantom.



**Figure 44:** Time-intensity curves of the four fibroglandular tissue ROIs and one tumour ROI for monitoring the contrast flushing out of the phantom after contrast administration.

In figure 45 only tumour ROI 3 and fibroglandular tissue ROI 2 are plotted, to show which result would be optimal to achieve for the distribution of contrast for every ROI. It can be seen that the tumour shows an immediate increase in the intensity value right after contrast administration and reaches the highest intensity at two seconds after starting the measurement, after which the intensity immediately drops. It can also be seen that ROI 2 reaches a higher intensity after the tumour already lost most of its intensity.



**Figure 45:** Time-intensity curve of fibroglandular tissue ROI 2 and tumour ROI 3.

## 7 Discussion

This section discusses the extent to which the phantoms meet the requirements, improvements that can be made to the current phantoms or protocols, and to what extent the results are consistent with literature.

The phantoms do not meet functional requirement II, since both phantoms contain air bubbles. This can possibly be solved by gently centrifuging the phantom until all air bubbles are driven to the surface, or by using a laboratory platform shaker and simultaneously tapping the phantom up and down for a longer time. The air can be removed from the tumour by injecting pressurised water through the tumour tubing and simultaneously rotating the phantom at different angles. The air may also be removed by placing the phantom in the high-pressure chamber. Removing the air is crucial for testing the phantoms on the dedicated Dynamic contrast-enhanced breast CT (DCE-bCT).

Tumour requirement III was not met because more than 20% of the contrast agent flowed through the fibroglandular tissue. This may be solved by using two inputs and two outputs, as discussed further below.

Besides these requirements, the phantoms meet all requirements. The location, shape, and size of the phantoms are based on the anatomical breast, the phantoms mimic perfusion of fibroglandular tissue by using sodium alginate beads, they are transparent, printed using SLA printing, they have a wall thickness of 1 mm, contain 1 input and 1 output, the phantoms are attached to the lid, are completely closed and watertight, fit inside the 'breast bucket' and the tumour made by S. Gouma [34] fits inside the fibroglandular tissue phantom.

The small cut in the bottom of the phantom with associated cap should be made larger to make it easier to fill the phantom with sodium alginate beads. Now, only a few beads fit through the hole and it takes about an hour to completely fill the phantom. Also, the small cap that needs to fit in this cut should be made about 7% smaller than the cut, to fit tightly into the cut. This 7% is based on the recommendation to make the cap diameter 7.5 mm for an 8 mm cut, as discussed in chapter 4.10.1.

As recommended in chapter 4.10.3, the tumour tubing can best be glued to the lid before filling the phantom, to ensure the phantom is completely watertight.

The fibroglandular tissue phantom shape and size is based on the average percentage of fibroglandular tissue in the anatomical breast at a specific location, however, these percentages differ per person. In the future, more phantoms with different fibroglandular tissue shapes and sizes can be made to accurately validate the DCE-bCT scanner with different kinds of breasts.

In the design of this phantom, sodium alginate beads are chosen to mimic perfusion in fibroglandular tissue, however, this is a simplified model of anatomical breast vascularity and could therefore be mimicked more accurately by using other techniques such as moulding with silicone. The sodium alginate beads now also play a major role in the shelf life of the phantom, as they consist of natural materials that go mouldy over time. When making the beads, it is very important to work hygienically, but this can only extend the durability for a limited time. It may, therefore, be useful to choose a different material for the filling of the phantom.

The wall of the phantom is made of solid resin and is, therefore, not deformable and elastic. In order to mimic the attenuation properties better, it can also be useful to make the wall of the phantom out of elastic materials such as gelatin [35].

To prevent the contrast from getting stuck in the bottom right corner of the phantoms and to make the contrast outflow better, a few improvements are considered.

During the imaging protocols in which iodine was used, instead of water, it is better to use glycerol to flush out the phantom so that the viscosity is the same as that of the contrast agent. This makes sure the iodine is more easily and quickly flushed out of the tumour and phantom. Another way to make this possible is to heat the iodinated contrast agent so that it becomes less viscous.

Another option is to adjust the shape of the phantom, by flattening the bottom right corner to make it impossible for contrast to get stuck there.

To make a quantitative comparison of the intensity values of the ROIs in the time-intensity curves, three things need to be taken into account.

First, the intensity must be corrected for the volume of the phantom, because the phantom does not have a uniform thickness and, therefore, the ROIs have different starting intensities. However, if the phantom is tested on the DCE-bCT, this is not a problem since the breast CT takes 3D images of the breast over time.

Also, the ROI of the tumour does not cover the entire tumour. As a result, the stationary contrast at the bottom of the tumour was not visible in the time-intensity curve. In further research, it is, therefore, better to consider the entire tumour as an ROI to enable better quantitative analysis.

Finally, there is a decrease in the intensity value in figures 43 and 45 in the fibroglandular tissue ROIs at  $t = 1$  s. This is caused by an automatic adjustment in the intensity value in the Artis Pheno C-arm when the contrast is administrated. To correct this, an ROI outside the fibroglandular tissue phantom can be used as a reference. The time-intensity curve of this ROI can then be subtracted from the existing time-intensity curve.

By using these three modifications, a better quantitative comparison can be made.

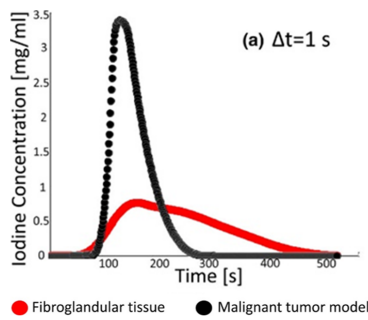


**Figure 46:** The difference in iodine concentration for the tumour and fibroglandular tissue ROI. [17]

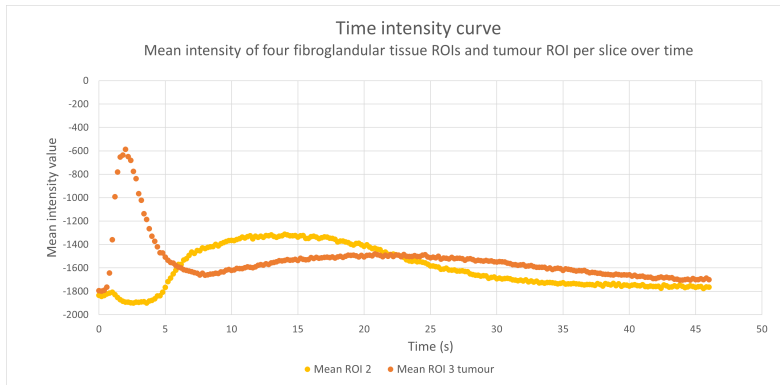


**Figure 47:** Time-intensity curve of the third and fourth ROI: a fibroglandular tissue ROI and the tumour ROI.

A previous digital phantom study showed the iodine concentration curves of a tumour and fibroglandular tissue, as can be seen in figure 46. The shape of the time-intensity curve in figure 47 corresponds to some extent to this figure. Although the time-intensity curve shows a later enhancement of the fibroglandular tissue ROI 4, compared to the tumour ROI, the tumour ROI does show a significantly higher intensity during the enhancement than the fibroglandular tissue ROI, which is equivalent to the shape of the iodine concentration curves. It can be useful to test whether fewer or more holes in the tumour tubing provide better or worse agreement with the contrast distribution and the ratio of tumour and fibroglandular tissue enhancement found in this previous study.

The iodine concentration curves in figure 46 show partial simultaneous enhancement of the tumour and fibroglandular tissue. However, the time-intensity curves in figure 47 do not show the enhancement simultaneously. This may be solved by allowing two separate fluid flows through the phantom to better regulate contrast flow. This requires two inputs and two outputs, one for the tumour and one for the fibroglandular tissue. This also allows more accurate mimicking of the 20/80 distribution of contrast agent, as discussed in tumour requirement III.

In the two figures above, it can also be seen that the increase in attenuation or iodine concentration over time differs significantly. In figure 46 the iodine concentration increases about a hundred seconds after contrast administration and this increase remains for about one hundred seconds, however, in figure 47 the attenuation increases already after one second and remains for about four seconds. This may be mimicked better by using a lower flow rate of the pump.

If the phantom shape and size are modified, it can be used for other imaging modalities, for example CEM and DCE-MRI, as mentioned in the introduction.

## 8 Conclusion

Two Fibroglandular Tissue Phantoms enhanced with perfusion capabilities, to simulate background parenchymal enhancement (BPE), have been developed successfully. The shape of the phantoms is based on the anatomical breast and the phantoms are filled with sodium alginate beads to mimic microvascular blood flow. The second phantom contained a tumour and tubing for the enhancement of both the fibroglandular tissue and tumour model. Contrast-enhanced dynamic imaging of this phantom shows time-intensity curves corresponding with the expected attenuation curves of a tumour and fibroglandular tissue in patients. The phantoms can be used for the validation and optimisation of the acquisition and reconstruction parameters for dynamic contrast-enhanced breast CT (DCE-bCT). The shape and size of the phantom could also be modified to be used for contrast-enhanced mammography or other imaging modalities.

## References

- [1] “Risk of breast cancer | RIVM,” June 2023. [Online; accessed 11. Jun. 2024].
- [2] E. T. Sedeta, B. Jobre, and B. Avezbakiyev, “Breast cancer: Global patterns of incidence, mortality, and trends.,” *Journal of Clinical Oncology*, vol. 41, no. 16\_suppl, pp. 10528–10528, 2023.
- [3] S. Törnberg, L. Kemetli, N. Ascunce, S. Hofvind, A. Anttila, B. Sèradour, E. Paci, C. Guldenfels, E. Azavedo, A. Frigerio, V. Rodrigues, and A. Ponti, “A pooled analysis of interval cancer rates in six European countries,” *Eur. J. Cancer Prev.*, vol. 19, pp. 87–93, Mar. 2010.
- [4] R. Meucci, C. A. Pistolese, T. Perretta, G. Vanni, E. Beninati, F. D. I. Tosto, M. L. Serio, A. Caliendo, M. Materazzo, M. Pellicciaro, and O. C. Buonomo, “Background Parenchymal Enhancement in Contrast-enhanced Spectral Mammography: A Retrospective Analysis and a Pictorial Review of Clinical Cases,” *In Vivo*, vol. 36, pp. 853–858, Mar. 2022.
- [5] M. L. Nock, M. P. Kempston, J. G. Mainprize, and M. J. Yaffe, “Quantitative flow phantom for contrast-enhanced breast tomosynthesis,” *Medical Imaging 2007: Physics of Medical Imaging*, vol. 6510, p. 65102W, Mar. 2007.
- [6] R. Vairavan, O. Abdullah, P. B. Retnasamy, Z. Sauli, M. M. Shahimin, and V. Retnasamy, “A Brief Review on Breast Carcinoma and Deliberation on Current Non Invasive Imaging Techniques for Detection,” *Curr. Med. Imaging Rev.*, vol. 15, no. 2, pp. 85–121, 2019.
- [7] N. Kiarashi and E. Samei, “Digital breast tomosynthesis: A concise overview,” *Imaging in Medicine*, vol. 5, pp. 467–476, 10 2013.
- [8] L. M. F. H. Neeter, H. P. J. F. Raat, R. Alcantara, Q. Robbe, M. L. Smidt, J. E. Wildberger, and M. B. I. Lobbes, “Contrast-enhanced mammography: what the radiologist needs to know,” *BJR Open*, vol. 3, no. 1, 2021.
- [9] D. Kontos, P. R. Bakic, A.-K. Carton, A. B. Troxel, E. F. Conant, and A. D. A. Maidment, “Parenchymal Texture Analysis in Digital Breast Tomosynthesis for Breast Cancer Risk Estimation: A Preliminary Study,” *Acad. Radiol.*, vol. 16, p. 283, Mar. 2009.
- [10] A. Elmi, E. F. Conant, A. Kozlov, A. J. Young, Q. Long, R. K. Doot, and E. S. McDonald, “Preoperative breast MR imaging in newly diagnosed breast cancer: Comparison of outcomes based on mammographic modality, breast density and breast parenchymal enhancement,” *Clin. Imaging*, vol. 70, p. 18, Feb. 2021.
- [11] I. Sechopoulos, “A review of breast tomosynthesis. Part I. The image acquisition process,” *Med. Phys.*, vol. 40, Jan. 2013.
- [12] D. Thomasson, Y. Pang, M. Bernardo, and P. L. Choyke, “The role of dynamic contrast-enhanced MRI in cancer diagnosis and treatment,” *Diagnostic and interventional radiology (Ankara, Turkey)*, vol. 16, p. 186, Nov. 2009.
- [13] P. L. Choyke, A. J. Dwyer, and M. V. Knopp, “Functional tumor imaging with dynamic contrast-enhanced magnetic resonance imaging,” *J. Magn. Reson. Imaging*, vol. 17, pp. 509–520, May 2003.
- [14] C. K. Kuhl, H. H. Schild, and N. Morakkabati, “Dynamic bilateral contrast-enhanced MR imaging of the breast: trade-off between spatial and temporal resolution,” *Radiology*, vol. 236, pp. 789–800, Sept. 2005.
- [15] C. K. Kuhl, P. Mielcareck, S. Klaschik, C. Leutner, E. Wardelmann, J. Gieseke, and H. H. Schild, “Dynamic breast MR imaging: are signal intensity time course data useful for differential diagnosis of enhancing lesions?,” *Radiology*, vol. 211, pp. 101–110, Apr. 1999.
- [16] M. A. Mafraji, “MSD Manual Professional Edition,” Nov. 2024. [Online; accessed 8. Nov. 2024].

- [17] M. Caballo, K. Michielsen, C. Fedon, and I. Sechopoulos, “Towards 4D dedicated breast CT perfusion imaging of cancer: development and validation of computer simulated images,” *Phys. Med. Biol.*, vol. 64, p. 245004., Dec. 2019.
- [18] J. J. Pautasso, M. Mikerov, L. Goris, K. Michielsen, and I. Sechopoulos, “4D dynamic contrast-enhanced breast CT: evaluation of quantitative accuracy,” in *Proceedings Volume 13174, 17th International Workshop on Breast Imaging (IWBI 2024)*, vol. 13174, pp. 208–212, SPIE, May 2024.
- [19] L. Goris, J. Pautasso, M. Mikerov, K. Michielsen, and I. Sechopoulos, “Perfusion phantom for the optimization of dynamic contrast-enhanced dedicated breast CT: iodine contrast curves in a simplified breast phantom,” in *Proceedings Volume 13174, 17th International Workshop on Breast Imaging (IWBI 2024)*, vol. 13174, pp. 195–200, SPIE, May 2024.
- [20] N. D. Prionas, K. K. Lindfors, S. Ray, S.-Y. Huang, L. A. Beckett, W. L. Monsky, and J. M. Boone, “Contrast-enhanced dedicated breast CT: initial clinical experience,” *Radiology*, vol. 256, pp. 714–723, Sept. 2010.
- [21] S. Wienbeck, U. Fischer, S. Luftner-Nagel, J. Lotz, and J. Uhlig, “Contrast-enhanced cone-beam breast-CT (CBBCT): clinical performance compared to mammography and MRI,” *Eur. Radiol.*, vol. 28, pp. 3731–3741, Sept. 2018.
- [22] “Izotropic Receives Patent to Measure Breast Density with Breast CT • APPLIED RADIOLOGY,” Sept. 2024. [Online; accessed 10. Sep. 2024].
- [23] M. Caballo, R. Mann, and I. Sechopoulos, “Patient-based 4D digital breast phantom for perfusion contrast-enhanced breast CT imaging,” *Med. Phys.*, vol. 45, pp. 4448–4460, Oct. 2018.
- [24] C. K. Kuhl, “MRI of breast tumors,” *Eur. Radiol.*, vol. 10, no. 1, pp. 46–58, 2000.
- [25] M. J. Yaffe and N. F. Boyd, “Quantitative Image Analysis for Estimation of Breast Cancer Risk,” in *Handbook of Medical Image Processing and Analysis (Second Edition)*, pp. 381–398, Cambridge, MA, USA: Academic Press, Jan. 2009.
- [26] D. Safarian, “Breast Density: Understanding its Significance and Impact on Breast Health,” *Consulting Radiologists*, Aug. 2024.
- [27] C. Fedon, M. Caballo, E. García, O. Diaz, J. M. Boone, D. R. Dance, and I. Sechopoulos, “Fibroglandular tissue distribution in the breast during mammography and tomosynthesis based on breast CT data: A patient-based characterization of the breast parenchyma,” *Med. Phys.*, vol. 48, pp. 1436–1447, Mar. 2021.
- [28] S.-Y. Huang, J. M. Boone, K. Yang, N. J. Packard, S. E. McKenney, N. D. Prionas, K. K. Lindfors, and M. J. Yaffe, “The characterization of breast anatomical metrics using dedicated breast CT,” *Med. Phys.*, vol. 38, pp. 2180–2191, Apr. 2011.
- [29] S. Vedantham, L. Shi, K. E. Michaelsen, V. Krishnaswamy, B. W. Pogue, S. P. Poplack, A. Karel-las, and K. D. Paulsen, “Digital breast tomosynthesis guided near infrared spectroscopy: volumetric estimates of fibroglandular fraction and breast density from tomosynthesis reconstructions,” *Biomed. Phys. Eng. Express*, vol. 1, p. 045202, Oct. 2015.
- [30] Y. Ma, A. Liu, Y. Zhang, Y. Zhu, Y. Wang, M. Zhao, Z. Liang, Z. Qu, L. Yin, H. Lu, and Z. Ye, “Comparison of background parenchymal enhancement (BPE) on contrast-enhanced cone-beam breast CT (CE-CBBCT) and breast MRI,” *Eur. Radiol.*, vol. 32, pp. 5773–5782, Aug. 2022.
- [31] O. S. University. [Online; accessed 10. Sep. 2024].
- [32] M. Ducci, “Figure 3. alginate beads have a shell consisting of calcium alginate sparingly soluble in water : Redox reactions in sodium alginate beads,” 2019. [Online; accessed 10. Sep. 2024].
- [33] D. W. Abueidda, M. Elhebeary, C.-S. A. Shiang, S. Pang, R. K. Abu Al-Rub, and I. M. Jasiuk, “Mechanical properties of 3d printed polymeric gyroid cellular structures: Experimental and finite element study,” *Materials and Design*, vol. 165, p. 107597, 2019.

- [34] S. Gouma, "Design and testing of a breast perfusion tumor phantom for dynamic contrast-enhanced computed tomography," bachelor's thesis, University of Twente, 2024.
- [35] E. Dahal, A. Badal, A. Zidan, A. Alayoubi, and B. Ghammraoui, "Stable gelatin-based phantom materials with tunable x-ray attenuation properties and 3D printability for x-ray imaging," *Phys. Med. Biol.*, vol. 63, May 2018.

## A Appendix: Generative AI disclosure

During the preparation of this work, the author used LanguageTool and Overleaf spell check to check the spelling and grammar, and BibTeX to list the references in Overleaf. After using this tool/service, the author thoroughly reviewed and edited the content as needed, taking full responsibility for the final outcome.